

pubs.acs.org/Macromolecules Article

Quantifying the Effect of Multivalent Ions in Polyelectrolyte Solutions

Michael Jacobs, Carlos G. Lopez, and Andrey V. Dobrynin*



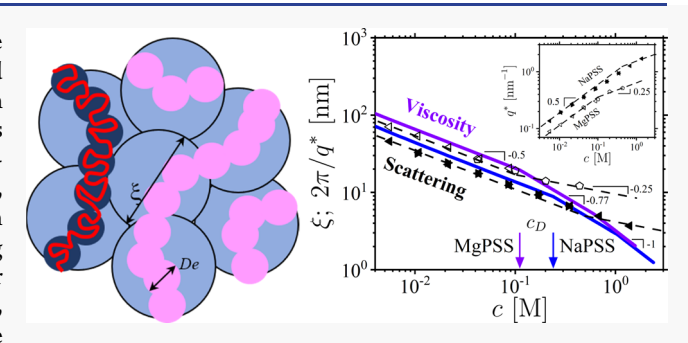
Cite This: Macromolecules 2021, 54, 9577-9586



ACCESS

Metrics & More

ABSTRACT: We implemented a scaling approach, based on the relationship between the solution correlation length $\xi = lg^{\nu}/B$ and the number of repeat units per correlation blob g for polymers with repeat unit projection length l, to quantify properties of solutions of carboxymethylcellulose and polystyrene sulfonate with monovalent and divalent counterions. The parameter B is equal to $B_{\rm pe}$, $B_{\rm g}$, $B_{\rm th}$, and 1, and the exponent $\nu = 1$, 0.588, 0.5, and 1 in semidilute polyelectrolyte solutions, solutions of overlapping electrostatic and thermal blobs, and concentrated polymer solutions, which are separated by crossover concentrations $c_{\rm D}$, $c_{\rm th}$, and c^{**} , respectively. The values of the B-parameters are



Article Recommendations

obtained using the linear relationship between the specific viscosity $\eta_{\rm sp}(c)$ in the unentangled solution regime and the number of correlation blobs $N_{\rm w}/g$ per chain, with the weight-average degree of polymerization, $N_{\rm w}$, and $g=B^{3/(3\nu-1)}(cl^3)^{1/(1-3\nu)}$ as a function of the repeat unit concentration, c, and the B-parameters in different solution regimes. This analysis shows that (i) there is only a small fraction of free counterions, $f^* < 12\%$; (ii) divalent ions have a strong effect on the renormalization of the excluded volume, reducing it by a factor of 2; and (iii) the effect of divalent counterions is much weaker on the renormalization of the Kuhn length, accounting for an increase of up to 10%. In combination, these effects significantly reduce chain stretching, increase the number of repeat units per solution correlation length, and promote chain disentanglement in polyelectrolyte solutions with divalent ions in comparison with that in solutions with monovalent counterions. There is an indication of chain bridging by Ca^{2+} ions in concentrated solutions of carboxymethylcellulose, manifested as an increase in solution viscosity. The concentration dependence of the solution correlation length ξ calculated using the set of B-parameters is in good agreement with that obtained from the peak position of the scattering function for concentrations $c < c_D$.

INTRODUCTION

Divalent counterions can significantly alter the behavior of polyelectrolyte solutions. $^{1-20}$ In salt-free solutions, they are more effective in screening the charge of polyelectrolytes by doubling the contribution to the solution ionic strength in comparison with their monovalent counterparts. 21 This efficient screening weakens electrostatic interactions between ionized groups, reduces chain size, and shifts the semidilute solution regime toward a higher concentration range. In addition to charge screening, divalent ions are more susceptible to counterion condensation due to a lower entropy penalty for ion localization around the charged polymer backbone.²¹ Condensed divalent ions mediate the attraction between polyelectrolytes, forcing their collapse and precipitation with increasing polymer concentration—effectively worsening solvent quality for the polymer backbone. This ability of multivalent ions is used by nature in the condensation of DNA for packaging inside cells and viruses.^{3,22,23} At high polymer concentrations, divalent ions can play the role of physical crosslinks, bridging polyelectrolyte chains together. ^{4,7,9} This leads to the formation of reversible physical networks, which is

manifested by a dramatic increase in the solution viscosity in a narrow concentration range. 4,20

Despite significant experimental, ^{2-4,10,11,13-20} computational, ²⁴⁻²⁹ and theoretical ^{1,5-9,12,30-32} efforts, a quantitative description of polyelectrolyte solutions with divalent counterions continues to be desired. Here, we will address this issue by applying a recently developed data analysis technique ^{33,34} to evaluate scaling parameters, describing the conformations of polyelectrolyte and neutral chains at different length scales. The method ^{33,34} is based on the linear dependence of the solution specific viscosity on the weight-average degree of polymerization and the concentration dependence of the solution correlation length in the unentangled solution regime.

Received: June 20, 2021 Revised: September 13, 2021 Published: October 6, 2021





In particular, we apply this scaling approach^{33,34} to obtain the fraction of ionized groups, excluded volume, and Kuhn length in salt-free solutions of carboxymethylcellulose (CMC) with Na⁺, Ca²⁺, Mg²⁺, Mn²⁺, Co²⁺, and Ba²⁺ counterions^{18,35} and polystyrene sulfonate with Na⁺ and Mg²⁺ counterions.^{36–39} This information is used to elucidate the differences and similarities in the system behavior depending on the counterion valence. Furthermore, this approach^{33,34} allows us to represent solution specific viscosity as a universal function of the number of repeat units per solution correlation length in a broad concentration range.

The rest of the paper is organized as follows. We begin with a brief overview of the scaling model of salt-free polyelectrolyte solutions and illustrate how to quantify the scaling relations and to find numerical coefficients connecting the size of the solution correlation blob with the number of repeat units in it. After that, we apply this approach to calculate the fraction of localized counterions, excluded volume, and Kuhn length in salt-free solutions of CMC and polystyrene sulfonate with different types of counterions. For each system, the results of the scaling analysis for the solution correlation length based on the solution viscosity are compared with those obtained from scattering experiments. Finally, we will show how to use the developed approach to quantify the effect of counterion valence on counterion condensation, excluded volume, and Kuhn length and present a picture of polyelectrolyte solutions supported by our findings.

SCALING MODEL

In our analysis of the viscosity of semidilute salt-free polyelectrolyte solutions in the presence of multivalent counterions, we extend a scaling approach developed in recent publications. This approach is based on the relationship between the correlation length (blob size) ξ and the number of the repeat units in it, g, with projection length l^{40-42}

$$\xi = \lg^{\nu}/B \tag{1}$$

The numerical coefficient B and exponent v are determined by the solvent quality for the polymer backbone and the type and strength of interactions at different length scales, starting from the solution correlation length down to the chain Kuhn length b and repeat unit projection length l. In semidilute polyelectrolyte solutions, the exponent v=1, 0.588, 0.5, and 1, and the B-parameter is equal to $B_{\rm pe}$, $B_{\rm g}$, $B_{\rm th}$, and 1 in the different solution regimes, reflecting that correlation blobs are made of electrostatic blobs with sizes $D_{\rm e}$ and number of repeat units $g_{\rm e}$, which in turn contain thermal blobs each of size $D_{\rm th}$ and number of repeat units $g_{\rm th}$ (Figure 1a).

In particular, on the length scales r smaller than the Kuhn length b but larger than or equal to the projection length, $l \le r$ < b, a section of the chain is rod-like with a linear relationship between the number of repeat units g_r and its size

$$r = lg_r$$
, for $l \le r < b$ (2)

This corresponds to the values of B=1 and exponent v=1. Within a thermal blob, on the length scales $b \le r < D_{\rm th}$, the chain statistics is that of a random walk of Kuhn segments such that

$$r = (lbg_r)^{0.5} = lg_r^{0.5}/B_{th}, \text{ for } b \le r < D_{th}$$
 (3)

where the parameter

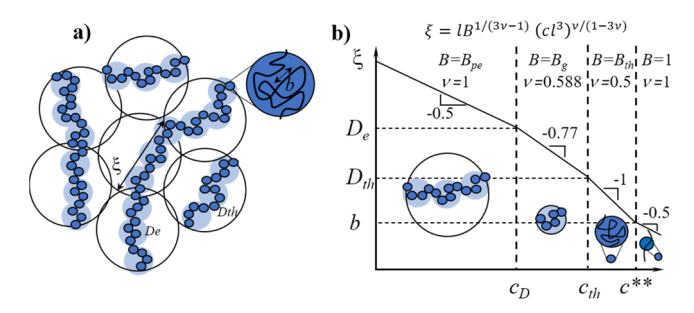


Figure 1. (a) Schematic representation of the hierarchy of length scales in semidilute salt-free polyelectrolyte solutions. (b) Concentration dependence of the solution correlation length in salt-free polyelectrolyte solutions for $c > c^*$. $c_{\rm D}$ —electrostatic blob overlap concentration, $c_{\rm th}$ —thermal blob overlap concentration, and c^{**} —crossover concentration to the concentrated solution regime. Insets show the chain structure on the length scales of the correlation length. Logarithmic scales. Adapted from ref 33. Copyright ACS 2021.

$$B_{\rm th} = (l/b)^{0.5} \tag{4}$$

is always smaller than unity, and the exponent v = 0.5.

Excluded volume interactions determine chain behavior on the length scales $D_{\rm th} < r \le D_{\rm e}$. At these length scales, the chain statistics is that of a self-avoiding walk of thermal blobs

$$r = D_{\text{th}} (g_{\text{r}}/g_{\text{th}})^{0.588} = lg_{\text{r}}^{0.588}/B_{\text{g}}, \text{ for } D_{\text{th}} \le r < D_{\text{e}}$$
 (5)

Thus, the exponent $\nu = 0.588$, and the parameter $B_{\rm g}$ describes the swelling of the chain within the electrostatic blob. It can be expressed in terms of the repeat unit excluded volume ν , Kuhn length b, and projection length l as follows

$$B_{\rm g} = B_{\rm th} (\nu/(lb)^{1.5})^{1-2\nu} \tag{6}$$

The last equation immediately follows from the Flory expression for the chain size when it is rewritten for an arbitrary exponent ν . Note that the value of the parameter $B_{\rm g}$ could be larger or smaller than unity, depending on the ratio of $\nu/(lb)^{1.5}$ and the value of the parameter $B_{\rm th}$.

Finally, on the length scales $D_e \le r < \xi$, electrostatic repulsion between ionized groups results in chain stretching

$$r = D_{\rm e}g_{\rm r}/g_{\rm e} = lg_{\rm r}/B_{\rm pe}, \text{ for } D_{\rm e} \le r < \xi \tag{7}$$

which corresponds to the exponent v=1. The parameter $B_{\rm pe}$ is related to the number of repeat units $g_{\rm e}$ per electrostatic blob with size $D_{\rm e}^{~33}$

$$B_{\rm pe} = lg_{\rm e}/D_{\rm e} \tag{8}$$

It is larger than unity and describes the tension in the chain of electrostatic blobs.

The space-filling condition of correlation blobs (the repeat unit concentration inside the blobs is equal to the solution concentration)

$$c = g/\xi^3 \tag{9}$$

provides expressions for the correlation length

$$\xi = lB^{1/(3\nu - 1)}(cl^3)^{\nu/(1 - 3\nu)} \tag{10}$$

and the number of polymer repeat units per correlation volume

$$g = B^{3/(3\nu-1)} (cl^3)^{1/(1-3\nu)}$$
(11)

as functions of the concentration of repeat units. This is illustrated in Figure 1b with crossover concentrations between

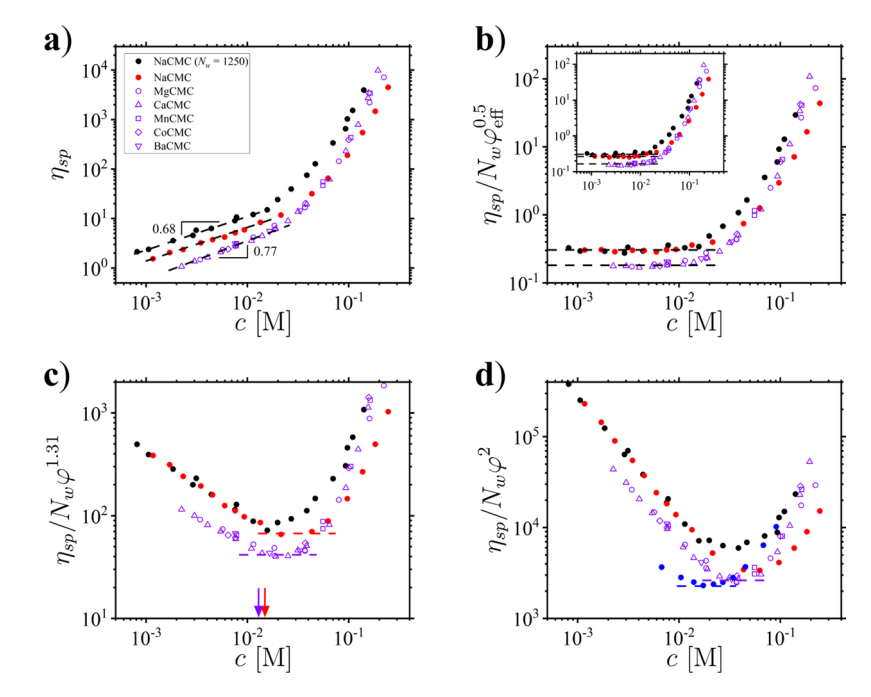


Figure 2. (a) Dependence of the specific viscosity $\eta_{\rm sp}=(\eta-\eta_{\rm s})/\eta_{\rm s}$ and normalized specific viscosity (b) $\eta_{\rm sp}/N_{\rm w}\varphi_{\rm eff}^{0.5}$ (inset shows plots with original $N_{\rm w}=820$), (c) $\eta_{\rm sp}/N_{\rm w}\varphi^{1.31}$, and (d) $\eta_{\rm sp}/N_{\rm w}\varphi^2$ on concentration of repeat units c in solutions of NaCMC, MgCMC, CaCMC, MnCMC, CoCMC, and BaCMC with the corrected weight-average degree of polymerization $N_{\rm w}=720$ (red and violet symbols) and $N_{\rm w}=1250$ (black circles) and repeat unit projection length l=0.515 nm. Dimensionless concentration $\varphi=cl^3$. Lines and arrows of different colors (b-d) show crossover concentrations and plateau values used for calculations of the B-parameters. (d) Blue circles correspond to NaCMC with $N_{\rm w}=1250$ in 2 M NaCl from ref 33.

different solution regimes: $c_{\rm D}$ —electrostatic blob overlap concentration, $c_{\rm th}$ —thermal blob overlap concentration, and c^{**} —crossover concentration to the concentrated solution regime.

In polyelectrolyte solutions with low salt concentrations, there is an additional screening of electrostatic interactions by added monovalent salt ions with concentration c_s , which results in the following renormalization of the solution correlation length 6,42,43

$$\xi = lB_{\rm pe}^{0.5} (cl^3)^{-0.5} (1 + 2c_{\rm s}/zf^*c)^{0.25}$$
(12)

In writing eq 12, we take into account that the counterions have valence z and f^* is the fraction of ionized groups on the polymer backbone. The expression in the brackets in the r.h.s. of eq 12 is a ratio of the ionic strength of a solution due to counterions with valence z and monovalent salt ions $I(c_s) = zf^*c + 2c_s$ to the ionic strength of counterions $I(0) = zf^*c$ in a salt-free solution. Note that in writing the expression for the contribution of multivalent counterions to the ionic strength, we use the electroneutrality condition for the concentrations of free multivalent ions c_Z and ionized groups f^*c_s , such that $zc_Z = f^*c_s$.

In the framework of the scaling model of dynamics of semidilute solutions, it is postulated that the screening of hydrodynamic interactions between chains takes place at the length scale $\xi_{\rm H}$, which is proportional to the solution correlation length, $\xi_{\rm H} \approx \xi_{\rm .}^{40,44-47}$ This assumption results in the solution specific viscosity $\eta_{\rm sp}$ in both the Rouse and entangled solution regimes to be given by the following crossover expression 33

$$\eta_{\rm sp} = N_{\rm w} \left(1 + \frac{N_{\rm w}}{N_{\rm e}} \right)^2 \begin{cases} g^{-1}, & \text{for } c \le c^{**} \\ cbl^2, & \text{for } c^{**} < c \end{cases}$$
(13)

where $N_{\rm w}$ is the weight-average degree of polymerization and $N_{\rm e}$ is the number of repeat units per entanglement strand, which scales with concentration as follows ^{33,48,49}

$$N_{\rm e} = \tilde{P}_{\rm e}^2 \begin{cases} g, & \text{for } c \le c^{**} \\ c^{-2} (lb)^{-3}, & \text{for } c^{**} < c \end{cases}$$
 (14)

In eq 14, $\tilde{P}_{\rm e}$ is the number of entangled strands (packing number) required for a section of a chain with $N_{\rm e}$ repeat units to entangle. We use " $\tilde{...}$ " to indicate that the system polydispersity is included in the definition of the packing number. ^{33,34} Accounting for the different concentration scaling of the number of repeat units per correlation blob g and strand degree of polymerization $N_{\rm e}$ in the concentrated solution regime $c > c^{**}$ requires rescaling the specific viscosity by a factor of $\lambda = clb^2 = c/c^{**}$ for $c > c^{**}$ and rewriting eq 9 as ³³

$$\lambda \eta_{\rm sp} = \frac{N_{\rm w}}{g} \left(1 + \frac{N_{\rm w}}{\tilde{P}_{\rm e}^2 g} \right)^2 \tag{15}$$

The number of repeat units g per blob is calculated using eq 11 for $c \le c^{**}$, and $g = B_{\text{th}}^{-2}(c^{**}/c)^2$ for $c > c^{**}$.

The numerical values of the *B*-parameters are obtained by taking into account that in the Rouse regime (see eq 15), the solution specific viscosity, $\eta_{\rm sp}$, is equal to the number of blobs per chain, $\eta_{\rm sp}=N_{\rm w}/g$. This points out that the specific viscosity scales with the concentration of repeat units as $c^{1/(3\nu-1)}$ in accordance with eq 11. Thus, a normalized specific viscosity $\eta_{\rm sp}/N_{\rm w}(cl^3)^{1/(3\nu-1)}$ with the scaling exponent ν determined by the chain statistics on the length scale of the correlation blob

should have a plateau regime or flat minima from the location of which we can extract the corresponding crossover concentrations (c_D and c_{th}) and values of the *B*-parameters.³³ In the next section, we apply this approach to obtain *B*-parameters in polyelectrolyte solutions with monovalent and multivalent counterions.

DATA ANALYSIS AND DISCUSSION

Carboxymethylcellulose. We begin analysis of the effect of divalent ions on properties of polyelectrolyte solutions of CMC with repeat unit projection length l=0.515 nm. Figure 2a shows the concentration dependence of the solution viscosity for aqueous solutions of CMC with different counterions Na⁺, Ca²⁺, Mg²⁺, Mn²⁺, Co²⁺, and Ba²⁺, the weight-average degree of polymerization $N_{\rm w}=820$ and degree of substitution DS ≈ 1.3 for the red and violet symbols, ¹⁸ and $N_{\rm w}=1250$ and DS $=1.2\pm0.1$ for the black circles. ³⁵ It follows from the specific viscosity plots in Figure 2a that the specific viscosity increases faster than $\eta_{\rm sp}\sim c^{0.5}$, indicating the presence of residual salt. We account for this effect by using the low-salt version of the solution correlation length (see eq 12). With this modification, in order to obtain the value of the parameter $B_{\rm pe}$, in the inset of Figure 2b, we normalize specific viscosity data by a factor $N_{\rm w}\varphi_{\rm eff}^{0.5}$ in which

$$\varphi_{\text{eff}}^{0.5} = \varphi^{0.5} (1 + 2c_{s}/zf^{*}c)^{-0.75}$$
(16)

with $\varphi = cl^3$ being the dimensionless concentration of repeat units and the ratios of salt concentration and fraction f^* of free counterions $c_s/f^* = 3.3 \times 10^{-4} \text{ M}$ and $2.0 \times 10^{-3} \text{ M}$ for NaCMC and CMC systems with divalent counterions, respectively. This normalization results in two distinct plateaus for the short and long chains, suggesting different values of the $B_{\rm pe}$ parameter as shown in the inset. However, the overlapping values of DS and c_s/f^* for both NaCMC systems suggest that these two systems should have similar plateaus. To collapse the data, we adjusted the degree of polymerization of the short chains from the initial weight-average degree of polymerization $N_{\rm w}$ = 820 to $N_{\rm w}$ = 720 to match the plateau location with that for the system with longer chains $N_{\rm w}$ = 1250, as shown on the main graph in Figure 2b. This correction of the molecular weight results in plateaus located at $C_p = 0.305$ and $C_p = 0.181$ for monovalent and divalent counterions, respectively. This gives the corresponding values of $B_{\rm pe} = C_{\rm p}^{-2/3} = 2.21$ and $B_{\rm pe} =$

The values of the parameters $B_{\rm g}$ describing chain statistics on the length scales of the electrostatic blob were estimated from the intermediate concentration range plateaus shown in Figure 2c as $B_{\rm g} = C_{\rm p}^{-0.255}$, resulting in $B_{\rm g} = 0.35$ for sodium counterions and $B_{\rm g} = 0.39$ for the divalent counterions. Likewise, values of the parameter $B_{\rm th}$ are obtained from the minimum in Figure 2d as $B_{\rm th} = 0.28$ for NaCMC and $B_{\rm th} = 0.27$ for divalent CMCs. The difference between values of $B_{\rm g}$ is about 10%, while values of $B_{\rm th}$ are very close. The close values of $B_{\rm th}$ indicate that the solvent packing around the backbone controls the chain rigidity, while the effect of counterion valence is insignificant.

With this information in hand, in Figure 3, we replot the normalized specific viscosity data in terms of the number of correlation blobs per chain $N_{\rm w}/g$. For this figure, the concentration dependence of the number of repeat units per correlation length g was calculated by substituting the obtained values of the B-parameters and $c_{\rm s}/f^*$ (see Table 1) into the

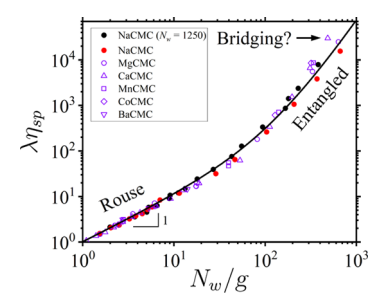


Figure 3. Dependence of normalized specific viscosity $\lambda\eta_{\rm sp}$ on the number of blobs per chain $N_{\rm w}/g$ for aqueous solutions of NaCMC, MgCMC, CaCMC, MnCMC, CoCMC, and BaCMC with a weight-average degree of polymerization $N_{\rm w}=720$ (red and violet symbols) and $N_{\rm w}=1250$ (black circles) and repeat unit projection length of 0.515 nm. Multiplication factor $\lambda=1$ for $c\leq c^{**}$, and $\lambda=c/c^{**}$ for $c^{**}< c$. The number of repeat units per correlation blob is calculated using eq 7 for $c\leq c^{**}$ and $g=B_{\rm th}^{-2}(c^{**}/c)^2$ for $c>c^{**}$. The solid line corresponds to the best fit to eq 15 with fitting parameter $\tilde{P}_{\rm e}=11.4$.

expression $g=c\xi^3$ with ξ given by eqs 10 and 12. In this representation, all datasets mostly collapse into a single universal curve, confirming the assumption of the scaling model that solution specific viscosity is a universal function of the number of correlation blobs per chain (eq 15) and is independent of the chain conformations inside a blob. This means that semidilute solutions of chains with different degrees of polymerization could have the same solution specific viscosity and yet be in different solution regimes as long as the number of correlation blobs per chain remains the same. The data collapse in Figure 3 also serves as an ultimate test of our approach in determining the *B*-parameters used in the calculations of the number of repeat units per correlation blob, *g*.

We can identify two characteristic regimes in the dependence of the specific viscosity on the number of blobs per chain. For a small number of blobs $N_w/g < 40$, the specific viscosity increases linearly with the number of blobs N_w/g , which corresponds to unentangled (Rouse) chain dynamics. Around $N_{\rm w}/g \approx 100$ blobs, the data show a clear deviation from the linear scaling, and one can argue that the systems begin to cross over into the entangled solution regime with $\lambda \eta_{\rm sp} \sim (N_{\rm w}/$ g)³. Fitting the data to eq 13 results in packing number \tilde{P}_{e} = 11.4. This value of the packing number is slightly larger than the value $\tilde{P}_{e} = 9.7$ reported in ref 33. This change in the packing number \tilde{P}_e can be attributed to the additional datasets with different degrees of polymerization and better accuracy in the evaluation of the B_{σ} -parameter. Using the packing number $ilde{P}_{
m e}$, we can estimate the number of blobs per chain that is needed for a chain of blobs to entangle, $N_e/g \approx \tilde{P}_e^2 \approx 130$. Thus, in solutions with monovalent and divalent counterions, chains with $N_{\rm w}$ = 720 entangle at concentrations $c_{\rm e} \approx 0.11~{\rm M}$ and $c_{\rm e} \approx 0.10$ M, respectively.

It is important to point out that the CaCMC system appears to demonstrate a faster increase in the specific viscosity with the number of blobs per chains in comparison with other systems, which cannot be accounted for by the error in the determination of $N_{\rm w}/g$. This could be due to intermolecular association between two CMC chains that are bridged together by ${\rm Ca^{2+}}$ ions. This bridging increases the effective chain degree of polymerization. We can estimate the degree of polymerization of an aggregate by moving the last point to the best-fit line. This analysis results in $N_{\rm w,eff} \approx 1020$. Note that the

Table 1. Summary of the System Parameters^a

system	$N_{ m w}$	c_s/f^* [M]	B_{pe}	$D_{\rm e}$ [nm]	$g_{\rm e}$	$c_{\mathrm{D}} [\mathrm{M}]$	B_{g}	D_{th} [nm]	$g_{ m th}$	$c_{\mathrm{th}} [\mathrm{M}]$	$B_{ m th}$	<i>b</i> [nm]	c^{**} [M]
NaCMC	1250	3.3×10^{-4}	2.2	21	94	0.016	0.35	6.8	13	0.070	0.28	6.8	0.070
NaCMC	720	3.3×10^{-4}	2.2	21	94	0.016	0.35	6.8	13	0.070	0.28	6.8	0.070
$X^{2+}CMC$	720	2.0×10^{-3}	3.1	29	189	0.013	0.39	15	62	0.030	0.27	7.1	0.064
NaPSS	125-740	4.0×10^{-4}	2.9	8.8	100	0.24	0.43	2.9	15	1.04	0.34	2.2	1.35
NaPSS	1400-4600	0.0	2.2	7.9	69	0.23	0.39						
MgPSS	125-4600	3.0×10^{-4}	6.6	20	517	0.11	0.50	5.0	50	0.65	0.36	2.0	1.6

"The table entries are calculated using the following expressions: crossover concentrations: c_D was obtained numerically from $B_p{}^{0.5}(c_Dl^3)^{(1-\nu)/(6\nu-2)}(1+2c_s/zf^*c_D)^{0.25}=B_g^{1/(3\nu-1)},\ c_{\rm th}=B_{\rm th}^3(B_{\rm th}/B_g)^{1/(2\nu-1)}/l^3,\ {\rm and}\ c^{**}=B_{\rm th}^4/l^3;\ {\rm electrostatic}\ {\rm blob}\ {\rm size}\ D_{\rm e}=lg_{\rm e}^{\nu}/B_{\rm g},\ {\rm thermal}\ {\rm blob}\ {\rm size}\ D_{\rm th}=lg_{\rm th}^{0.5}/B_{\rm th};\ {\rm number}\ {\rm of}\ {\rm repeat}\ {\rm units}\ {\rm per}\ {\rm electrostatic}\ {\rm blob}\ g_{\rm e}=(B_g^3/c_Dl^3)^{1/(3\nu-1)};\ {\rm number}\ {\rm of}\ {\rm repeat}\ {\rm units}\ {\rm per}\ {\rm thermal}\ {\rm blob}\ g_{\rm th}=(B_g/B_{\rm th})^{2/(2\nu-1)};\ {\rm sumber}\ {\rm of}\ {\rm repeat}\ {\rm units}\ {\rm per}\ {\rm thermal}\ {\rm blob}\ g_{\rm th}=(B_g/B_{\rm th})^{2/(2\nu-1)};\ {\rm of}\ {\rm o$

observed difference in solution specific viscosity $\eta_{\rm sp}$ as a function of $N_{\rm w}/g$ between systems with Ca²⁺ and Mg²⁺ ions could be due to the ions' relative strengths in the Hofmeister series (i.e., Ca²⁺ > Mg²⁺) in promoting associations in aqueous solutions. ⁵⁰

Finally, we compare the solution correlation length estimated from the analysis of the viscosity data with the ones obtained in the scattering experiments^{51,52} shown in Figure 4. For this figure, the concentration dependence of the

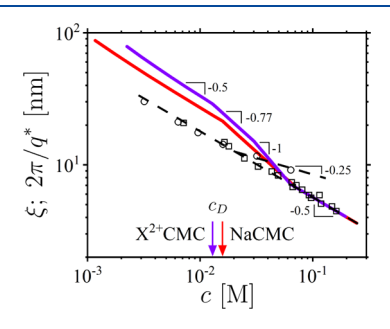


Figure 4. Correlation length ξ as a function of concentration for aqueous solutions of NaCMC, (red line), MgCMC, CaCMC, MnCMC, CoCMC, and BaCMC (violet line) with a repeat unit projection length of 0.515 nm. Open black symbols show $2\pi/q^*$ for NaCMC with $N_{\rm w}=720$ (circles) and 1250 (squares), where q^* corresponds to peak positions obtained in the SAXS and SANS experiments in refs 51 and 52, respectively. Arrows point to locations of crossover concentration $c_{\rm D}$.

correlation length of the CMC systems was calculated by substituting the obtained values of the *B*-parameters (see Table 1) into eqs 10 and 12. For the concentration range below the electrostatic blob overlap concentration, $c < c_D$, electrostatic interactions are dominant, and the correlation length is given by eq 12. At very low concentrations of the repeat units, the effect of the residual salt is significant, resulting in a deviation from the expected salt-free scaling dependence of the solution correlation length, $\xi \sim c^{-0.5}$. In the concentration intervals $c_D < c < c_{\rm th}$ and $c_{\rm th} < c < c^{**}$, we substituted the values of the parameter $B = B_{\rm g}$ and $B = B_{\rm th}$ in eq 6. Finally, in the concentrated solution regime $c > c^{**}$, the correlation length $\xi \approx (cl)^{-0.5}$.

In the concentration interval $c < c_D$, the calculated correlation length is larger than the correlation length $\xi \approx 2\pi/q^*$ obtained from the scattering peak position q^* determined in the small-angle X-ray scattering (SAXS) experiments for $N_{\rm w}=720$ systems (see Figure 4). This value is proportional to the correlation length with a

proportionality coefficient of 1.5. The concentration dependence of the length scale corresponding to $2\pi/q^*$ has a crossover at $c\approx 0.02$ M to a regime with $2\pi/q^*\approx c^{-0.25}$. At this concentration range, the peak in the scattering function correlates with the characteristic length scale of the charge density fluctuations, ⁵³ which is different from the solution correlation length ξ . Note that this crossover concentration is consistent with $c_{\rm D}\approx 0.016$ M estimated from the viscosity data.

However, the analysis of the small-angle neutron scattering (SANS) data so shows that the scaling for the length scale $2\pi/q^* \sim c^{-0.5}$ continues past $c_{\rm D}$, all the way through the concentrated solution regime, serendipitously overlapping with the calculated correlation length in the concentration interval c^* (see Figure 4). It is unclear what causes the difference between SANS and SAXS results for q^* in the concentration range $c_{\rm D} < c$. so $c^{51,52}$

Table 1 summarizes all the parameters for the CMC systems obtained from the analysis of the viscosity data.

Polystyrene Sulfonate (PSS). We extend the approach developed above to quantify the effect of divalent ions on solution properties of polystyrene sulfonate. Figure 5 shows the analysis of viscosity data for sodium polystyrene sulfonate (NaPSS) with six different molecular weights ranging from 2.9×10^4 to 9.7×10^5 g/mol.^{26,27} The degrees of polymerization were determined from the molecular weights of the parent polystyrene samples divided by the molar mass of the polystyrene repeat unit, $M_0 = 104$ g/mol. The repeat unit projection length for a carbon backbone is l = 0.255 nm. At low concentrations, the specific viscosity data shown in Figure Sa scale with concentration as $\eta_{\rm sp}\sim c^{0.58}$ for solutions of chains with $N_{\rm w}=740$, indicating some level of residual salt, while the samples with $N_{\rm w}$ = 1400 show no such deviation from the electrostatics-dominated salt-free scaling regime $\eta_{\rm sp} \sim c^{0.5}$. In particular, for datasets with $N_{\rm w} \leq 740$, $c_{\rm s}/f^*$ was estimated to be 4×10^{-4} M. To improve the data overlap within each group, we have corrected $N_{\rm w}$ and shown the corrected values in bold with the original $N_{\rm w}$ values shown in brackets. These $N_{\rm w}$ corrections are within 20%. Analysis of the data in Figure 5c,d is done similarly to the CMC systems with the obtained values of the B_{σ} and B_{th} parameters summarized in Table 1.

The separation of the datasets into two sets of curves indicates that the actual sulfonation degrees of these samples are different. In particular, this variation in the degree of sulfonation would affect the chain Kuhn length (and thus $B_{\rm th}$), solvent quality for the polymer backbone, a determining value of the parameter $B_{\rm g}$, and the strength of the electrostatic interactions on the length scale of the electrostatic blob size

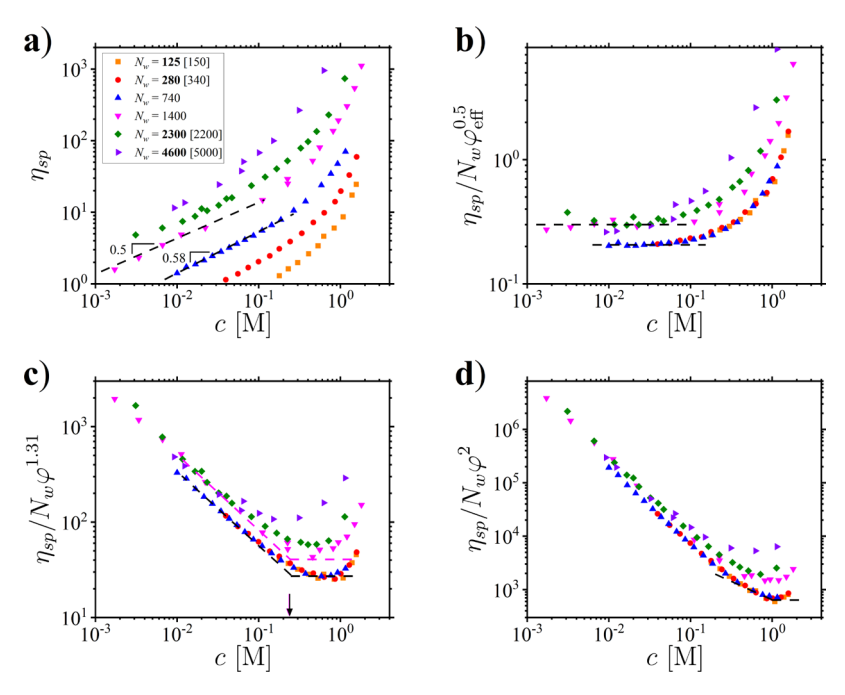


Figure 5. Concentration dependence of specific viscosity $\eta_{\rm sp}$ (a) and reduced specific viscosity $\eta_{\rm sp}/N_{\rm w}\varphi_{\rm eff}^{0.5}$ (b), $\eta_{\rm sp}/N_{\rm w}\varphi^{1.31}$ (c), and $\eta_{\rm sp}/N_{\rm w}\varphi^2$ (d) of aqueous solutions of sodium polystyrene sulfonate (NaPSS). Dashed lines and colored arrows (b–d) indicate plateau values and crossover concentrations used in calculations of the *B*-parameters, respectively. Dimensionless concentration $\varphi = cl^3$. Results of analysis are summarized in Table 1.

described by parameter B_{pe} . This manifests in the existence of the different plateaus in Figure 5b-d.

Figure 6 shows the solution specific viscosity data in terms of the number of correlation blobs per chain. Once again, we can

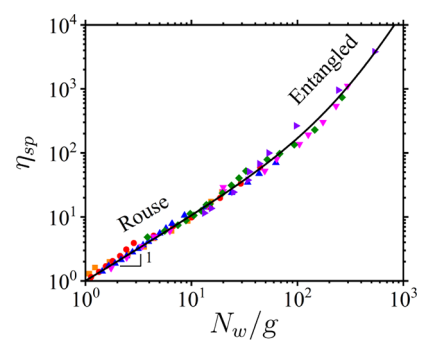


Figure 6. Specific viscosity $\eta_{\rm sp}$ as a function of the number of correlation blobs per chain, $N_{\rm w}/g$. The solid line corresponds to the best fit to eq 15 with the fitting parameter $\tilde{P}_{\rm e}=18$. Symbol notations are the same as in Figure 5.

clearly identify the two different scaling regimes of Rouse and entangled chain dynamics. Fitting the data to eq 15 results in $\tilde{P}_{\rm e} \approx 18$. We can use the relationship $N_{\rm e}/g \approx \tilde{P}_{\rm e}^{\ 2} \approx 324$ and estimate the entanglement concentration in solutions of chains with $N_{\rm w} = 4600$ as $c_{\rm e} \approx 0.78$ M.

The same NaPSS samples were then used to prepare and study MgPSS solutions in ref 39. Figure 7a shows specific viscosity data taken from this study with the same adjusted values of $N_{\rm w}$ as ones used for NaPSS. The largest-molecular weight samples show a concentration dependence of $\eta_{\rm sp} \sim c^{0.57}$, indicating the existence of residual salt, which we estimate to be $c_{\rm s}/f^*=3\times 10^{-4}$ M. The data in Figure 7b–d are compiled to perform analysis similar to the NaPSS systems, with the results summarized in Table 1.

Figure 8 shows the dependence of specific viscosity on the number of correlation blobs per chain $N_{\rm w}/g$. The data are almost entirely in the Rouse regime, only deviating from $\eta_{\rm sp} = N_{\rm w}/g$ around $N_{\rm w}/g \approx 60$. For reference, we have added the same curve as in Figure 6. The overlap of this curve with the data suggests that the divalent MgPSS systems have a similar value of \tilde{P}_e as the monovalent NaPSS systems.

As in the case of the CMC systems, we can overlay the calculated values of the correlation length ξ with experimental values obtained from the peak position $2\pi/q^*$. For this plot, we use values for scattering peak positions q^* given in refs 15, 16, 39, and 54. These data are shown in Figure 9, with arrows indicating our estimations for the locations of the electrostatic blob overlap concentration c_D for NaPSS and MgPSS solutions (see Table 1). As in Figure 4, there is a constant shift factor between our viscosity measurements of ξ and $2\pi/q^*$, approximately equal to 1.2. In the inset, the peak position data q^* are plotted as a function of concentration. Based on the location of the crossover between $q^* \sim c^{0.5}$ and $q^* \sim c^{0.25}$ concentration regimes, the estimated values of c_D for the MgPSS and NaPSS systems are 0.10 and 0.35 M, respectively. Thus, crossover concentrations between different solution regimes determined using both techniques are consistent.

Counterion Condensation and the Structure of Polyelectrolyte Solutions. Using the results presented in Table 1, we can estimate what fraction of counterions f^* is able to escape the electrostatic blobs and what fraction remains inside the electrostatic blobs, reducing the effective charge of the polyelectrolyte chains. In the framework of the scaling approach, the electrostatic blob size $D_{\rm e}$ or the number of repeat units per blob $g_{\rm e}$ is determined by the conditions that the electrostatic energy of the blob with charge valence $f^*g_{\rm e}$ is on the order of the thermal energy $k_{\rm B}T$ ($k_{\rm B}$ is the Boltzmann constant and T is the absolute temperature) and chain statistics on the length scales smaller than the blob size is unperturbed

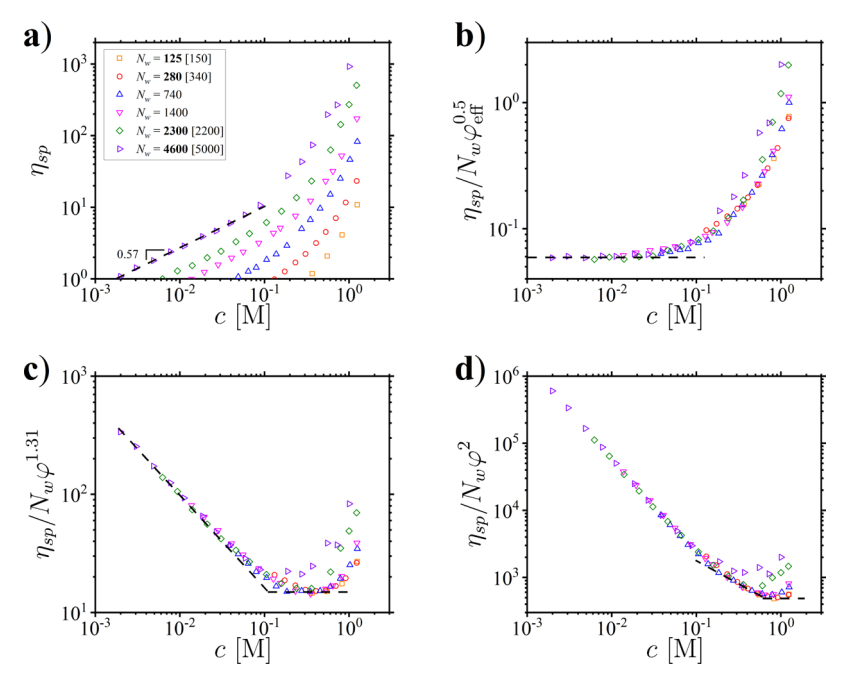


Figure 7. Concentration dependence of specific viscosity $\eta_{\rm sp}$ (a) and reduced specific viscosity $\eta_{\rm sp}/N_{\rm w}\varphi_{\rm eff}^{0.5}$ (b), $\eta_{\rm sp}/N_{\rm w}\varphi_{\rm eff}^{1.31}$ (c), and $\eta_{\rm sp}/N_{\rm w}\varphi^2$ (d) of aqueous solutions of magnesium polystyrene sulfonate (MgPSS). Dashed lines (b–d) indicate plateau values used to calculate the *B*-parameters. Dimensionless concentration of repeat units $\varphi = cl^3$. Results of analysis are summarized in Table 1. Data are from ref 39.

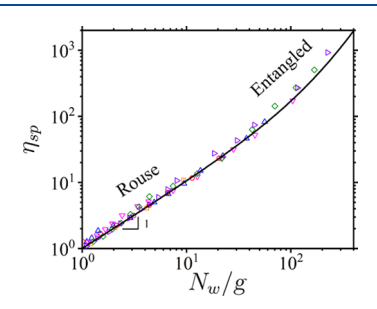


Figure 8. Specific viscosity $\eta_{\rm sp}$ as a function of the number of correlation blobs per chain, $N_{\rm w}/g$. The solid line corresponds to eq 15 with the value $\tilde{P}_{\rm e}=18$. Symbol notations are the same as in Figure 7.

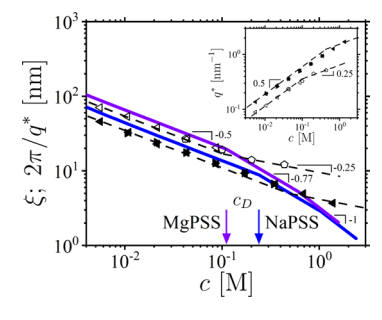


Figure 9. Concentration dependence of correlation length ξ for NaPSS with $N_{\rm w} \leq 740$ (blue line) and MgPSS (violet line) and $2\pi/q^*$ for the scattering peak position q^* (black symbols). Correlation length data are calculated using eqs 10 and 12 with the *B*-parameters given in Table 1. Filled left and right black triangles correspond to scattering data of NaPSS from refs 15, 16, and 54. Open left black triangles correspond to scattering data of CaPSS from ref 15. Open black pentagons correspond to scattering data of MgPSS from ref 39. The inset shows original peak position data. Arrows point to locations of crossover concentration $c_{\rm D}$.

by the electrostatic interactions. Due to the ambiguity in the definition of the electrostatic blob energy, we set this value

equal to $4k_BT$ and use this relationship to estimate the fraction of escaped (free) counterions as follows^{41,42}

$$\frac{l_{\rm B}f^{*2}g_{\rm e}^{\ 2}}{D_{\rm e}} \approx 4 \Rightarrow f^* \approx 2g_{\rm e}^{\ -1}(D_{\rm e}/l_{\rm B})^{0.5} \tag{17}$$

where $l_{\rm B}$ is the Bjerrum length, which is equal to $l_{\rm B}=0.7$ nm in aqueous solutions at room temperature. This selection of the electrostatic blob energy results in the fraction $f^* = 0.116$ of free counterions for NaPSS being close to the value estimated from osmotic pressure measurements $f^* \approx 0.16$. Repeating similar calculations for other systems, we find that f^* varies between 2 and 12% (see Table 2). For the same type of polymer backbones, the systems with divalent ions have a smaller fraction of free counterions. Thus, a significant fraction of counterions is localized inside the electrostatic blobs, as illustrated in Figure 10. This is an unexpected result, which, however, is consistent with the concentration dependence of the solution viscosity and the location of the crossover concentration to the concentrated polyelectrolyte solution regime observed in scattering experiments. It also could shed light on why scattering from polyelectrolyte solutions at concentrations below the electrostatic blob overlap concentration, $c < c_D$, provides a good estimate for the solution correlation length. In scattering experiments, counterions localized within the electrostatic blobs play the role of a natural contrast for the chains of blobs. When the electrostatic blobs overlap, the correlation between the solution correlation length and the charge density fluctuations decouples. It is important to point out that it is impossible to say with the information at hand how the counterions are distributed inside the electrostatic blobs. Are they condensed on the charged groups or localized within electrostatic blobs freely moving along the backbones? Addressing this question will require further investigations.

We can check what values of the counterion condensation parameter correspond to such low fractions of the free

Table 2. Counterion Condensation and Excluded Volume Parameter

system	$N_{ m w}$	z	$D_{ m e}$ [nm]	g_{e}	f^*	β	<i>b</i> [nm]	$\nu \ [nm^3]$
NaCMC	720	1	21	94	0.118	0.36	6.8	1.77
$X^{2+}CMC$	720	2	29	189	0.068	0.62	7.1	0.89
NaPSS	125-740	1	8.8	100	0.071	0.56	2.2	0.11
NaPSS	1400-4600	1	7.9	69	0.097	0.59		
MgPSS	125-4600	2	20	517	0.02	0.75	2.0	0.052

"The table entries are calculated according to the following procedures: the fraction of free counterions f^* is estimated using eq 17 and Bjerrum length $l_{\rm B} = 0.7$ nm; the counterion condensation parameter β is calculated from eq 18; and excluded volume ν is obtained from eq 19.

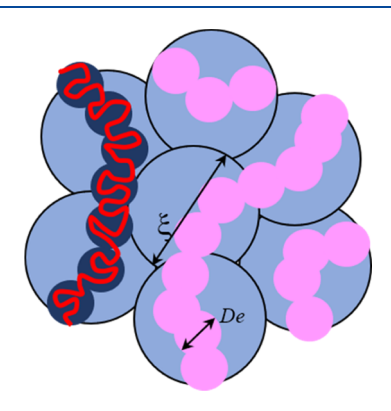


Figure 10. Schematic representation of the charge distribution in salt-free polyelectrolyte solutions. Lighter colors correspond to lower charge densities. High charge density on the polyelectrolyte chain is partially compensated by counterion density inside electrostatic blobs with size $D_{\rm e}$. The remaining counterions are distributed outside electrostatic blobs with complete charge compensation occurring on the length scales of the solution correlation length ξ .

counterions. The condensation parameter β is defined as the ratio of the magnitude of the energy of electrostatic attraction of a counterion with valence z on the surface of the electrostatic blob to the thermal energy $k_{\rm B}T^{21,56-59}$

$$\beta \approx z l_{\rm B} f^* g_{\rm e} / D_{\rm e} \tag{18}$$

Values of this parameter vary between 0.36 and 0.75 (see Table 2). Note that this estimate does not account for the contribution from correlation-induced attraction due to the redistribution of the charged groups on the polymer backbone and localized counterions, which should make the condensation parameter even larger.

The effect of the divalent ions on the renormalization of the Kuhn length is weak and accounts only for up to a 10% change in the PSS systems. This points to the solvation of the backbone as a dominant factor for the Kuhn length renormalization. We can use the obtained values of the Kuhn length to quantify the effect of multivalent ions on the repeat unit excluded volume by solving eq 6 for ν

$$\nu = (lb)^{3/2} (B_{\rm th}/B_{\rm g})^{1/(2\nu-1)}$$
(19)

using the *B*-parameters from Table 1 and substituting the good solvent exponent $\nu = 0.588$. The results of these calculations are presented in Table 2. This analysis shows that divalent ions reduce the excluded volume by a factor of 2, indicating a stronger screening of the electrostatic interactions.

CONCLUSIONS

We use a scaling approach to quantify the effect of divalent counterions on properties of aqueous solutions of CMC- and PSS-based polyelectrolytes. Our analysis shows that a significant fraction of counterions resides inside the electrostatic blobs with only a small fraction $f^* < 0.12$ filling the space between the chains (see Table 2). There are more condensed divalent counterions than one would expect. In both systems, the condensation of divalent ions results in a significant increase in the number of repeat units per electrostatic blob, a decrease in the chain tension, and the disentanglement of polyelectrolyte chains (see Table 1). There appears to be a stronger increase in solution viscosity in the CMC systems with divalent Ca^{2+} counterions, which could be attributed to the counterion-induced association of the chains at high polymer concentrations. This is illustrated in Figure 11,

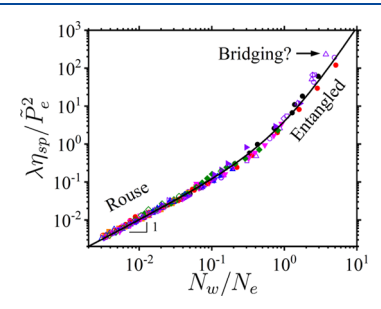


Figure 11. Dependence of normalized specific viscosity $\lambda\eta_{\rm sp}/\tilde{P}_{\rm e}^2$ on the number of entanglements per chain $N_{\rm w}/N_{\rm e}$, with $N_{\rm e}$ given by eq 14, for datasets in Figures 3, 6, and 8. The solid black line is given by $\lambda\eta_{\rm sp}/\tilde{P}_{\rm e}^2=(N_{\rm w}/N_{\rm e})(1+N_{\rm w}/N_{\rm e})^2$ with a multiplication factor $\lambda=1$ for $c\leq c^{**}$ and $\lambda=c/c^{**}$ for $c< c^{**}$.

showing a combined plot of normalized viscosity for all datasets discussed in this paper. Note that the observed difference between the viscosity of CMC systems with Ca^{2+} and Mg^{2+} counterions could be attributed to the difference of these counterions in promoting associations according to the Hofmeister series. ⁵⁰

Furthermore, divalent counterions have a strong effect on the renormalization of the excluded volume ν responsible for the swelling of chain sections inside electrostatic blobs. For both systems, it decreases by a factor of 2 in polyelectrolyte solutions with divalent ions in comparison with that in solutions with Na⁺ counterions (see Table 2). However, the effect of the divalent ions on the polymer Kuhn length is less dramatic, only accounting for less than 10% increase (see Table 1). For all studied systems, the calculated values of the solution correlation length at concentrations below the electrostatic blob overlap concentration, $c < c_D$, using the parameters presented in Table 1, are consistent with those observed in the scattering experiments, as illustrated in Figures 4 and 9.

Thus, our approach is shown to be very efficient in quantifying the effect of multivalent ions using only solution viscosity data. Furthermore, this analysis can also be used to

correct reported weight-average molecular weights and to estimate the fraction of free counterions. We hope that, considering the advantages of the developed technique and its simplicity, it will find a broad application in the analysis of solutions of charged and neutral polymers.

AUTHOR INFORMATION

Corresponding Author

Andrey V. Dobrynin — Department of Chemistry, University of North Carolina, Chapel Hill, North Carolina 27599-3290, United States; orcid.org/0000-0002-6484-7409; Email: avd@email.unc.edu

Authors

Michael Jacobs — Department of Chemistry, University of North Carolina, Chapel Hill, North Carolina 27599-3290, United States; © orcid.org/0000-0002-7255-3451

Carlos G. Lopez – Institute of Physical Chemistry, RWTH Aachen University, Aachen 52056, Germany; orcid.org/0000-0001-6160-632X

Complete contact information is available at: https://pubs.acs.org/10.1021/acs.macromol.1c01326

Notes

The authors declare no competing financial interest.

ACKNOWLEDGMENTS

This work was supported by the National Science Foundation under the grant DMREF-2049518. C.G.L. acknowledges funding from the DFG (grant number: GO 3250/2-1).

REFERENCES

- (1) de la Cruz, M. O.; Belloni, L.; Delsanti, M.; Dalbiez, J. P.; Spalla, O.; Drifford, M. Precipitation of highly charged polyelectrolyte solutions in the presence of multivalent salts. *J. Chem. Phys.* **1995**, *103*, 5781–5791.
- (2) Drifford, M.; Dalbiez, J.-P.; Delsanti, M.; Belloni, L. Structure and dynamics of polyelectrolyte solutions with multivalent salts. *Ber. Bunsenges. Physik. Chem.* **1996**, *100*, 829–835.
- (3) Bloomfield, V. A. DNA condensation by multivalent cations. *Biopolymers* **1997**, 44, 269–282.
- (4) Rubinstein, M.; Dobrynin, A. V. Associations leading to formation of reversible networks and gels. *Curr. Opin. Colloid Interface Sci.* 1999, 4, 83–87.
- (5) Shklovskii, B. I. Screening of a macroion by multivalent ions: Correlation-induced inversion of charge. *Phys. Rev. E: Stat. Phys., Plasmas, Fluids, Relat. Interdiscip. Top.* **1999**, *60*, 5802–5811.
- (6) Dobrynin, A.; Rubinstein, M. Theory of polyelectrolytes in solutions and at surfaces. *Prog. Polym. Sci.* **2005**, *30*, 1049–1118.
- (7) Ermoshkin, A. V.; Olvera de la Cruz, M. Polyelectrolytes in the presence of multivalent ions: Gelation versus segregation. *Phys. Rev. Lett.* **2003**, *90*, 125504.
- (8) Ermoshkin, A. V.; Olvera De La Cruz, M. Gelation in strongly charged polyelectrolytes. *J. Polym. Sci., Part B: Polym. Phys.* **2004**, 42, 766–776
- (9) Ermoshkin, A. V.; Kudlay, A. N.; Olvera de la Cruz, M. Thermoreversible crosslinking of polyelectrolyte chains. *J. Chem. Phys.* **2004**, *120*, 11930–11940.
- (10) Dubois, E.; Boué, F. Conformation of poly(styrenesulfonate) polyions in the presence of multivalent ions: Small-angle neutron scattering experiments. *Macromolecules* **2001**, *34*, 3684–3697.
- (11) Horkay, F.; Tasaki, I.; Basser, P. J. Effect of monovalent-divalent cation exchange on the swelling of polyacrylate hydrogels in physiological salt solutions. *Biomacromolecules* **2001**, *2*, 195–199.

- (12) Grosberg, A. Y.; Nguyen, T. T.; Shklovskii, B. I. Colloquium: The physics of charge inversion in chemical and biological systems. *Rev. Mod. Phys.* **2002**. *74*. 329–345.
- (13) Huang, C.-I.; Olvera de la Cruz, M. Polyelectrolytes in Multivalent Salt Solutions: Monomolecular versus Multimolecular Aggregation. *Macromolecules* **2002**, 35, 976–986.
- (14) Lages, S.; Lindner, P.; Sinha, P.; Kiriy, A.; Stamm, M.; Huber, K. Formation of Ca²⁺ induced intermediate necklace structures of polyacrylate chains. *Macromolecules* **2009**, *42*, 4288–4299.
- (15) Combet, J.; Isel, F.; Rawiso, M.; Boué, F. Scattering functions of flexible polyelectrolytes in the presence of mixed valence counterions: condensation and scaling. *Macromolecules* **2005**, *38*, 7456–7469.
- (16) Combet, J.; Rawiso, M.; Rochas, C.; Hoffmann, S.; Boué, F. Structure of polyelectrolytes with mixed monovalent and divalent counterions: SAXS measurements and Poisson—Boltzmann analysis. *Macromolecules* **2011**, *44*, 3039—3052.
- (17) Horkay, F.; Basser, P. J.; Hecht, A.-M.; Geissler, E. Chondroitin sulfate in solution: Effects of mono- and divalent salts. *Macromolecules* **2012**, *45*, 2882–2890.
- (18) Lopez, C. G.; Richtering, W. Influence of divalent counterions on the solution rheology and supramolecular aggregation of carboxylmethyl cellulose. *Cellulose* **2019**, *26*, 1517–1534.
- (19) Horkay, F.; Basser, P. J.; Hecht, A.-M.; Geissler, E. Ionic effects in semi-dilute biopolymer solutions: a small angle scattering study. *J. Chem. Phys.* **2018**, *149*, 163312.
- (20) Zhang, Z.; Chen, Q.; Colby, R. H. Dynamics of associating polymers. *Soft Matter* **2018**, *14*, 2961–2977.
- (21) Oosawa, F. Polyelectrolytes; Marcel Dekker, 1971.
- (22) Hayes, J. J.; Hansen, J. C. Nucleosomes and the chromatin fiber. Curr. Opin. Genet. Dev. 2001, 11, 124-129.
- (23) Belyi, V. A.; Muthukumar, M. Electrostatic origin of the genome packing in viruses. *Proc. Natl. Acad. Sci. U.S.A.* **2006**, *103*, 17174–17178.
- (24) Hsiao, P.-Y. Linear polyelectrolytes in tetravalent salt solutions. *J. Chem. Phys.* **2006**, *124*, 044904.
- (25) Hsiao, P.-Y. Chain morphology, swelling exponent, persistence length, like-charge attraction, and charge distribution around a chain in polyelectrolyte solutions: Effects of salt concentration and ion size studied by molecular dynamics simulations. *Macromolecules* **2006**, *39*, 7125–7137.
- (26) Klos, J.; Pakula, T. Lattice Monte Carlo simulations of a charged polymer chain: Effect of valence and concentration of the added salt. *J. Chem. Phys.* **2005**, *122*, 134908.
- (27) Lee, J.; Kim, S.; Chang, R.; Jayanthi, L.; Gebremichael, Y. Effects of molecular model, ionic strength, divalent ions, and hydrophobic interaction on human neurofilament conformation. *J. Chem. Phys.* **2013**, *138*, 015103.
- (28) Chremos, A.; Douglas, J. F. Influence of higher valent ions on flexible polyelectrolyte stiffness and counter-ion distribution. *J. Chem. Phys.* **2016**, *144*, 164904.
- (29) Shen, K.-H.; Fan, M.; Hall, L. M. Molecular dynamics simulations of ion-containing polymers using generic coarse-grained models. *Macromolecules* **2021**, *54*, 2031–2052.
- (30) Solis, F. J.; de la Cruz, M. O. Collapse of flexible polyelectrolytes in multivalent salt solutions. *J. Chem. Phys.* **2000**, *112*, 2030–2035.
- (31) Kundagrami, A.; Muthukumar, M. Theory of competitive counterion adsorption on flexible polyelectrolytes: Divalent salts. *J. Chem. Phys.* **2008**, *128*, 244901.
- (32) Muthukumar, M. 50th Anniversary Perspective: A Perspective on Polyelectrolyte Solutions. *Macromolecules* **2017**, *50*, 9528–9560.
- (33) Dobrynin, A. V.; Jacobs, M. When do polyelectrolytes entangle? *Macromolecules* **2021**, *54*, 1859–1869.
- (34) Dobrynin, A. V.; Jacobs, M.; Sayko, R. Scaling of polymer solutions as a quantitative tool. *Macromolecules* **2021**, *54*, 2288–2295.
- (35) Lopez, C. G.; Colby, R. H.; Graham, P.; Cabral, J. T. Viscosity and scaling of semiflexible polyelectrolyte NaCMC in aqueous salt solutions. *Macromolecules* **2017**, *50*, 332–338.

- (36) Lopez, C. G. Entanglement properties of polyelectrolytes in salt-free and excess-salt solutions. ACS Macro Lett. 2019, 8, 979–983.
- (37) Lopez, C. G. Scaling and entanglement properties of neutral and sulfonated polystyrene. *Macromolecules* **2019**, *52*, 9409–9415.
- (38) Lopez, C. G.; Richtering, W. Viscosity of semidilute and concentrated nonentangled flexible polyelectrolytes in salt-free solutions. *J. Phys. Chem. B* **2019**, 123, 5626–5634.
- (39) Lopez, C. G.; Horkay, F.; Schweins, R.; Richtering, W. Solution properties of polyelectrolytes with divalent counterions. *Macromolecules* **2021**. submitted.
- (40) Rubinstein, M.; Colby, R. H. *Polymer Physics*; Oxford University Press: New York, NY, 2003.
- (41) de Gennes, P. G.; Pincus, P.; Velasco, R. M.; Brochard, F. Remarks on polyelectrolyte conformation. *J. Phys.* **1976**, *37*, 1461–1473.
- (42) Dobrynin, A. V.; Colby, R. H.; Rubinstein, M. Scaling theory of polyelectrolyte solutions. *Macromolecules* **1995**, *28*, 1859–1871.
- (43) Dobrynin, A. V. Polyelectrolyte Solutions and Gels. In Oxford Handbook of Soft Matter; Terentjev, E., Weitz, D., Eds.; Oxford University Press: Oxford, 2015; pp 269–344.
- (44) de Gennes, P. G. Dynamics of entangled polymer solutions. I. The Rouse model. *Macromolecules* **1976**, *9*, 587–593.
- (45) de Gennes, P. G. Dynamics of entangled polymer solutions. II. Inclusion of hydrodynamic interactions. *Macromolecules* **1976**, *9*, 594–598.
- (46) de Gennes, P. G. Scaling Concepts in Polymer Physics; Cornell University Press: Ithaca, NY, 1979.
- (47) Doi, M.; Edwards, S. F. The Theory of Polymer Dynamics; Clarendon Press: Oxford, 1986.
- (48) Kavassalis, T. A.; Noolandi, J. New view of entanglements in dense polymer systems. *Phys. Rev. Lett.* **1987**, 59, 2674–2677.
- (49) Kavassalis, T. A.; Noolandi, J. Entanglement scaling in polymer melts and solutions. *Macromolecules* **1989**, *22*, 2709–2720.
- (50) Lo Nostro, P.; Ninham, B. W. Hofmeister phenomena: An update on ion specificity in biology. *Chem. Rev.* **2012**, *112*, 2286–2322.
- (51) Sharratt, W. N.; O'Connell, R.; Rogers, S. E.; Lopez, C. G.; Cabral, J. T. Conformation and phase behavior of sodium carboxymethyl cellulose in the presence of mono- and divalent salts. *Macromolecules* **2020**, *53*, 1451–1463.
- (52) Lopez, C. G.; Rogers, S. E.; Colby, R. H.; Graham, P.; Cabral, J. T. Structure of sodium carboxymethyl cellulose aqueous solutions: A SANS and rheology study. *J. Polym. Sci., Part B: Polym. Phys.* **2015**, 53, 492–501.
- (53) Borue, V. Y.; Erukhimovich, I. Y. A Statistical theory of weakly charged polyelectrolytes: Fluctuations, equation of state, and microphase separation. *Macromolecules* **1988**, *21*, 3240–3249.
- (54) Nishida, K.; Kaji, K.; Kanaya, T. High concentration crossovers in polyelectrolyte solutions. *J. Chem. Phys.* **2001**, *114*, 8671–8677.
- (55) Carrillo, J.-M.; Dobrynin, A. Salt effect on osmotic pressure of polyelectrolyte solutions: Simulation study. *Polymers* **2014**, *6*, 1897–1913.
- (56) Manning, G. S. Limiting laws and counterion condensation in polyelectrolyte solutions 1. Colligative properties. *J. Chem. Phys.* **1969**, 51, 924–933.
- (57) Manning, G. S. Polyelectrolytes. Annu. Rev. Phys. Chem. 1972, 23, 117–140.
- (58) Katchalsky, A. Polyelectrolytes. Pure Appl. Chem. 1971, 26, 327-374.
- (59) Katchalsky, A.; Alexandrowicz, Z.; Kedem, O. *Polyelectrolyte Solutions*; Conway, B. E., Barradas, R. G., Eds.; Wiley, 1966; pp 295–346.